

# Visual speech differentially modulates beta, theta, and high gamma bands in auditory cortex

Abbreviated Title: Multiple auditory responses to visual speech

Karthik Ganesan<sup>1</sup>, John Plass<sup>1</sup>, Adriene M. Beltz<sup>1</sup>, Zhongming Liu<sup>1</sup>, Marcia Grabowecky<sup>2</sup>, Satoru Suzuki<sup>2</sup>, William C. Stacey<sup>1</sup>, Vibhangini S. Wasade<sup>3,4</sup>, Vernon L. Towle<sup>5</sup>, James X Tao<sup>5</sup>, Shasha Wu<sup>5</sup>, Naoum P Issa<sup>5</sup>, David Brang<sup>\*1</sup>

<sup>1</sup>University of Michigan, Ann Arbor, MI 48109

<sup>2</sup>Northwestern University, Evanston, IL 60208

<sup>3</sup>Henry Ford Hospital, Detroit, MI 48202

<sup>4</sup>Department of Neurology, Wayne State University School of Medicine, MI 48201

<sup>5</sup>Department of Neurology, The University of Chicago, Chicago, IL 60637

\*Corresponding Author: [djbrang@umich.edu](mailto:djbrang@umich.edu)

## Page and Words Counts

32 Pages

8 Figures

1 extended data figure

Abstract: 225/250 words

Significance Statement: 116/120 words

Introduction: 598/650 words

Discussion: 1168/1500 words

## Conflict of Interest Statement

The authors declare no competing financial interests.

## Acknowledgements

This study was supported by NIH Grant R00 DC013828 A. Beltz was supported by the Jacobs Foundation. The authors report no conflicts of interest.

## Keywords

Multisensory; Audiovisual; Speech; ECoG; iEEG; sEEG; Intracranial

## **Significance Statement**

Visual speech cues are often needed to disambiguate distorted speech sounds in the natural environment. However, understanding how the brain encodes and transmits visual information for usage by the auditory system remains a challenge. One persistent question is whether visual signals have a unitary effect on auditory processing or elicit multiple distinct effects throughout auditory cortex. To better understand how vision modulates speech processing, we measured neural activity produced by audiovisual speech from electrodes surgically implanted in auditory areas of 21 patients with epilepsy. Group-level statistics using linear mixed-effects models demonstrated distinct patterns of activity across different locations, timepoints, and frequency bands, suggesting the presence of multiple audiovisual mechanisms supporting speech perception processes in auditory cortex.

## Abstract

Speech perception is a central component of social communication. While speech perception is primarily driven by sounds, accurate perception in everyday settings is also supported by meaningful information extracted from visual cues (e.g., speech content, timing, and speaker identity). Previous research has shown that visual speech modulates activity in cortical areas subserving auditory speech perception, including the superior temporal gyrus (STG), likely through feedback connections from the multisensory posterior superior temporal sulcus (pSTS). However, it is unknown whether visual modulation of auditory processing in the STG is a unitary phenomenon or, rather, consists of multiple temporally, spatially, or functionally discrete processes. To explore these questions, we examined neural responses to audiovisual speech in electrodes implanted intracranially in the temporal cortex of 21 patients undergoing clinical monitoring for epilepsy. We found that visual speech modulates auditory processes in the STG in multiple ways, eliciting temporally and spatially distinct patterns of activity that differ across theta, beta, and high-gamma frequency bands. Before speech onset, visual information increased high-gamma power in the posterior STG and suppressed beta power in mid-STG regions, suggesting crossmodal prediction of speech signals in these areas. After sound onset, visual speech decreased theta power in the middle and posterior STG, potentially reflecting a decrease in sustained feedforward auditory activity. These results are consistent with models that posit multiple distinct mechanisms supporting audiovisual speech perception.

## 1 Introduction

Auditory speech signals are conveyed rapidly during natural speech (3-7 syllables per second; Chandrasekaran et al., 2009), making the identification of individual speech sounds a computationally challenging task (Elliott and Theunissen, 2009). Easing the complexity of this process, audiovisual processes during face-to-face communication help predict and constrain perceptual inferences about speech signals in both a bottom-up and top-down manner (Bernstein and Liebenthal, 2014; Lewis and Bastiaansen, 2015; Peele and Sommers, 2015).

Multiple features extracted from visual signals can bias or enhance auditory speech perception processes, including lip shapes, rhythmic articulatory movements, and speaker identity, among others (Chandrasekaran et al., 2009; Erber, 1975; Chen and Rao, 1998; Van Wassenhove et al., 2005). While the net result is improved speech perception, each of these features may influence cortical auditory processes through distinct mechanisms. For example, visual speech is thought to influence the temporal structure of auditory speech processing by neurally amplifying auditory speech signals that are temporally correlated with lip closure, accomplished by modulating cortical excitability in auditory regions (Schroeder et al., 2008).

Indeed, functional dissociations are readily found in the auditory system. In the speech domain, previous research indicates that the STG exhibits an anterior-posterior gradient in feature tuning, with anterior regions being more sensitive to spectral content and posterior regions being more sensitive to temporal information (e.g., broadband amplitude dynamics) (Hullet et al., 2016). Because visual speech facilitates perception for both spectral details and temporal dynamics in speech (Plass et al., 2020), it could plausibly enhance perception through multiple distinct influences on STG areas specialized for different aspects of the auditory speech signal.

Importantly, prior research indicates that some audiovisual speech processes are associated with neural activity in distinct frequency bands, suggesting that they likely correspond to unique integrational functions across the sensory hierarchy (Arnal et al., 2009; Peele and Sommers, 2015). Consistent with previous observations of the distinct functions of “fast” and

“slow” oscillations throughout the perceptual system (Bastos et al., 2012), visual speech has been found to influence both theta and gamma oscillations associated with feedforward processing and beta oscillations associated with feedback signals (Arnal et al., 2009; Wang, 2010). These results suggest that visual speech likely influences both predictive and corrective components of auditory predictive coding through distinct neural mechanisms that operate at different timescales and levels of the neural hierarchy.

While fMRI studies have demonstrated broad activation of the STG during silent lipreading (Beauchamp et al., 2004a), this method does not provide information about the timing or spectral composition of these responses. Conversely, while intracranial electroencephalography (iEEG) provides substantially more temporal and spectral information, studies on audiovisual speech integration have largely focused on high-gamma power (HGp) indexes of local population firing rates, evaluated using single-participant statistics (e.g., Micheli et al., 2020; Besle et al., 2008), which severely limit inferences about normative neural processing. Here, we sought to examine visual effects on auditory speech processes across multiple frequency bands associated with both subthreshold oscillations and neural firing. Moreover, to integrate statistical results across participants, we used linear mixed-effects models to perform statistical inference at the group level, facilitating generalization.

To evaluate whether visual signals differentially modulate STG activity at distinct time scales, locations, and frequency bands, we recorded iEEG activity from a large group of patients ( $n = 21$ , 1367 electrodes in total) who performed an audiovisual speech task while undergoing clinical monitoring for epilepsy. Analyzing these data using group-level statistics, we found that visual speech produced multiple spatiotemporally distinct patterns of theta, beta, and high-gamma power throughout the STG. These results suggest that visual speech enhances auditory speech processes through multiple functionally distinct mechanisms.

## **2 Materials and Methods**

## 2.1 Participants, implants and recordings

Data were acquired from 21 patients with intractable epilepsy undergoing clinical evaluation using iEEG. Patients ranged in age from 15-58 years (mean = 37.1, SD = 12.8) and included 10 females. iEEG was acquired from clinically implanted depth electrodes (5 mm center-to-center spacing, 2 mm diameter) and/or subdural electrodes (10 mm center-to-center spacing, 3 mm diameter): 13 patients had subdural electrodes and 17 patients had depth electrodes (Extended Data 1-1). Across all patients, data was recorded from a total of 1367 electrodes (mean = 65, SD = 25.3, range = 24 - 131 per participant). The number, location, and type of electrodes used were based on the clinical needs of the participants. iEEG recordings were acquired at either 1000 Hz (n = 5), 1024 Hz (n = 11 participants), or 4096 Hz (n = 5 Participants) due to differences in clinical amplifiers. All participants provided informed consent under an institutional review board (IRB)-approved protocol at the University of Chicago, Rush University, University of Michigan, or Henry Ford hospital.

## 2.2 MRI and CT acquisition and processing

Preoperative T1-weighted magnetic resonance imaging (MRI) and a postoperative computed tomography (CT) scans were acquired for all participants. Registration of the preoperative MRI to postoperative CT was performed using statistical parametric mapping (SPM) and electrode localization was performed using custom software (Brang et al., 2016; available for download online <https://github.com/towle-lab/electrode-registration-app/>). This algorithm identifies and segments electrodes from the CT based on intensity values and projects subdural electrodes to the dura surface using the shape of the electrode disk to counteract postoperative compression. The Freesurfer image analysis suite (<http://surfer.nmr.mgh.harvard.edu/>; Dale, Fischl, and Sereno 1999; Fischl, Sereno, and Dale, 1999) was used for subsequent image processing procedures including cortical surface reconstruction, volume segmentation, and

anatomical labelling (<http://surfer.nmr.mgh.harvard.edu/>; Dale, Fischl, and Sereno 1999; Fischl, Sereno, and Dale, 1999).

### 2.3 Tasks and Stimuli

Participants were tested in the hospital at their bedside using a 15-inch MacBook Pro computer running Psychtoolbox (Kleiner et al., 2007). Auditory stimuli were presented through a pair of free-field speakers placed approximately 15 degrees to each side of the patient's midline, adjacent to the laptop. Data were aggregated from three audiovisual speech perception paradigms (using different phonemes spoken by different individuals across tasks) to ensure generalizability of results: 7 participants completed variant A, 8 participants variant B, and 6 participants variant C. Each task presented participants with auditory and visual speech stimuli in various combinations. As this study examines the modulatory role of visual information on auditory processes, only the auditory-alone and audiovisual (congruent) conditions were analyzed from each task variant.

On each trial a single phoneme was presented to the participant (variant A: /ba/ /da/ /ta/ /tha/, variant B: /ba/ /da/ /ga/, variant C: /ba/ /ga/ /ka/ /pa/). Figure 1 shows the timing and structure of an example trial from task variant B. Trials began with a fixation cross against a black screen that served as the intertrial interval (ITI), presented for an average of 750 ms (random jitter plus or minus 250 ms, uniformly sampled). In the audiovisual condition, the face appeared either 750

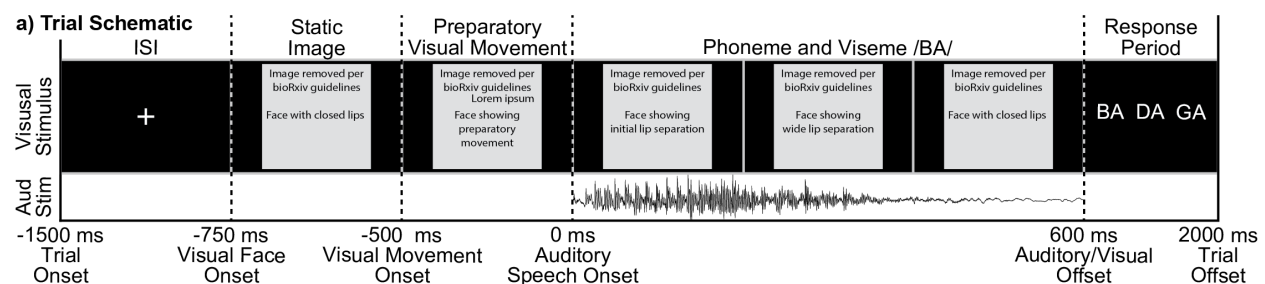


**Figure 1:** Task Variant B trial schematic. All trials began with a fixation cross 1500 ms before the onset of an auditory stimulus, lasting for an average of 750 ms (plus or minus 250 ms jitter). In the auditory-alone condition a blank screen followed the fixation cross for 750 ms. In the audiovisual condition the face appeared at the offset of the fixation (750 ms before sound onset), with preparatory visual movement beginning 250 ms later. Auditory phonemes (/ba/, /da/, or /ga/) onset at 0 ms in both conditions.

ms before sound onset (task variant B) or 500 ms before sound onset (variants A and C); across all three variants, face motion began at 500 ms before sound onset. In the auditory-alone condition, either the fixation cross persisted until sound onset (variant A) or a uniform gray square (mean contrast of the video images and equal in size) was presented for either 750 ms before sound onset (variant B) or 500 ms before sound onset (variant C). Following each trial participants were prompted to identify which phoneme they had heard either aloud or via button press. Trials were presented in a random order and phonemes were distributed uniformly across conditions. While conditions were matched in terms of trial numbers, participants completed a variable number of trials (based on task variant and the number of blocks completed): mean = 68 trials per condition (SD = 23, range = 32-96). Onset of each trial was denoted online by a voltage isolated TTL pulse.

## **2.4 iEEG Data Preprocessing**

All data were resampled to 1024 Hz during initial stages of processing for all participants. Data were referenced in a bipolar fashion (signals subtracted from each immediately adjacent electrode in a pairwise manner) to ensure that the observed signals were derived from maximally local neuronal populations. Noisy electrodes (variability in the raw signal greater than 5 SD compared to all electrodes) and noisy trials (variability in the raw signal greater than 3 SD across all trials within an electrode) were excluded from analyses. Slow drift artifacts and power-line interference were attenuated by high-pass filtering the data at .1 Hz and notch-filtering at 60 Hz (and its harmonics at 120, 180, and 240 Hz). Each trial was then segmented into a 2-second epoch centered around the onset of the trial. Individual trials were then separately filtered into three frequency ranges using wavelet convolution and then power transformed: theta (3 - 7 Hz, wavelet cycles varied linearly from 3-5), beta (13 - 30 Hz, wavelet cycles varied linearly from 5-10), HGp (70 - 150 Hz in 5 Hz intervals, wavelet cycles = 20 at 70 Hz, and increased linearly to maintain the same wavelet duration across frequencies).



Only electrodes meeting both anatomical and functional criteria were included in analyses. Anatomical selection required that an electrode be proximal to an auditory temporal lobe region as defined by the Freesurfer anatomical labels: "superiortemporal", "middletemporal", "supramarginal." Functional selection was evaluated separately for each of the three frequency bands of interest (theta, beta, and HGp) to identify auditory-responsive electrodes (such that different electrodes may be included across each of the frequency analyses). To ensure orthogonality with the examined condition differences, the functional localizer required electrodes to demonstrate a significant post-stimulus response (0 - 500 ms) regardless of condition relative to 0 using one-sample t-tests after correcting for multiple comparisons using false discovery rate (FDR). Beta and theta selection applied two-tailed t-tests while HGp applied one-tailed t-tests (as meaningful auditory HGp responses were predicted to elicit HGp increases).

## **2.5 Group-Level Analyses**

Traditionally, iEEG studies have focused on individual-participant analyses utilizing fixed-effect statistics (e.g., Micheli et al., 2018; Besle et al., 2008; Chang et al, 2010; Plass et al., 2019). While these approaches may be valid for estimating parameters and effect sizes within a single individual, they do not provide estimates across participants and thus lack generalizability across epilepsy patients, making inferences to the general population more difficult. Moreover, some studies mix between- and within-participant statistics by aggregating data from all participants without modeling participant as a random effect, violating independence assumptions (e.g., Lega, Germi, Rugg, 2017). This approach has been discussed extensively under the title of 'pseudoreplication' and can lead to spurious and poorly generalized results (for a discussion see Aarts et al., 2014; Lazic 2010; Lazic et al., 2018). These concerns for iEEG research have been raised and theoretically addressed previously by other groups using variants of a mixed-effects model (Kadipasoglu et.al., 2014; Kadipasoglu et al., 2015). To overcome these limitations, we employed two separate analysis approaches.

### **2.5.1 Group-Level Spatial Analyses**

To identify regions of the auditory temporal lobe that responded differently to auditory-alone versus audiovisual stimuli, we conducted individual-participant statistics and aggregated data across participants using an approach from the meta-analysis literature (treating each participant as an independent replication). Specifically, each 'virtual' bipolar electrode (calculated as the average coordinates between the associated pair of electrodes) was transformed into MNI space (Freesurfer `cvs_avg35_inMNI152`) and linked to neighboring vertices (within 10 mm Euclidean distance) on the Freesurfer MNI cortical pial surface (decimated from 1 mm to 4 mm); this one-to-many approach mitigates the imperfection of cross-subject spatial registration. Next, statistics were evaluated separately at each vertex for each participant using independent-sample t-tests, to compare auditory-alone and audiovisual trials between -1000 to 500 ms (auditory-onset at 0 ms; data were averaged across 100 ms time-windows prior to statistical analysis). Within-participant statistics were adjusted for multiple comparisons across vertices and time using FDR (Groppe, Urbach, and Kutas, 2011). The approach yielded individual-participant p-value maps at each of the 15 time-points. P-value maps were then aggregated across participants using Stouffer's Z-score method (Stouffer et al., 1949).

### **2.5.2 Group-Level Regional Time-Series Analyses**

While the meta-analysis approach establishes the strength of an effect at the group-level, it fails to provide group-level estimates and cannot effectively model data from both within and between participants (as is necessary in the evaluation of interactions across time, space, and analyzed frequency ranges). To model more general group differences between auditory-alone and audiovisual conditions we used linear mixed-effects models. As appropriately fitted models require more data than is often present at a single vertex, we created three regions of interest (ROIs) within the STG. ROIs were divided into three equal partitions from the "superiortemporal" label in Freesurfer, comprising anterior, middle, and posterior regions, similar to the division of

the STG used previously (Smith et al., 2013). Electrodes within 10 mm of these labels were linked to the closest of the three (no electrode was linked to multiple labels). Our focus on the STG was motivated by previous demonstrations of strong effects of lipreading in this region (e.g., Smith et al., 2013).

Linear mixed-effects modelling was performed using the `fitlme` function in Matlab R2019a (Mathworks Inc., Natwick, MA). Electrodes in the same ROI from the same participant were averaged prior to analysis to reduce the complexity of the model and as neighboring electrodes share variance. Individual trials were not averaged within or across participants prior to analysis. Nine main-effect models were constructed, in which differences between auditory-alone and audiovisual trials were separately evaluated at each of the three STG ROIs (anterior, middle, posterior) and three frequency bands (theta, beta, HGp) using the equation:

$$y_{ij} = \beta_0 + \beta_{1j} \text{participant}_{ij} + u_{0j} + \varepsilon_{ij}$$

Where,  $y$  represents the ECoG Trial Value, with a fixed effects term for the trial condition and a random intercept and slope term for the participant ID. In Matlab notation, this is represented as: `ECoG_Trial_Value ~ Trial_Cond + (Trial_Cond|Participant_ID)`. Critically, we modeled both random intercepts and random slopes for trial condition, as there were multiple measurements per participant and to maintain 'maximal' models for confirmatory hypothesis testing (Barr et al., 2013). Interaction models were subsequently constructed to evaluate whether audiovisual versus auditory-alone condition effects varied as a function of frequency band, ROI, and time, using the Matlab notation: `ECoG_Trial_Value ~ Trial_Cond * FrequencyBand * ROI * Time + (Trial_Cond|Participant_ID)`. While these model parameters were selected for inclusion based on confirmatory hypothesis testing, we also justified model selection using AIC comparisons. Separate models were constructed at each 1 ms time-point for the main-effect models. Data were averaged in 5 ms time-bins for the interaction models due to computational complexity and memory requirements. Statistics for the main-effect models were adjusted for

comparisons at multiple time-points from -500 to 500 ms using FDR correction ( $q = .05$ ) (Groppe, Urbach, and Kutas, 2011).

## 2.6 Individual Electrode Analyses

To examine individual differences in the patterns of activity evoked across electrodes and participants, individual electrode statistics were examined at representative electrodes. Unpaired t-tests were conducted separately at each time-point comparing audiovisual versus auditory HGp (random factor = trial). Statistics for the main-effect models were adjusted for comparisons at multiple time-points from -500 to 500 ms using FDR correction ( $q = .05$ ).

## 3 Results

### 3.1 Group-Level Spatial Analyses: Theta Power

Figure 2 shows group-level differences in theta power (3 - 7 Hz) between audiovisual and auditory-alone trials. A small but significant difference (audiovisual > auditory) emerged from -700 to -600 ms before sound onset in the supramarginal gyrus (peak coordinates:  $x = -60.7$ ,  $y = -56.2$ ,  $z = 30.3$ ,  $p = 0.0013$ ) with a peak-response in this region between -600 to -500 ms before sound onset (peak coordinates:  $x = -60.7$ ,  $y = -56.2$ ,  $z = 30.3$ ,  $p = 0.0003$ ). This activation pattern reflected only a small percentage of the supramarginal gyrus (SMG) (1.7% of SMG vertices at time-point -700 to -600 ms, and 2.6% of SMG vertices at time-point -600 to -500 ms). In contrast to this initial pattern, the majority of condition differences were observed in the middle temporal gyrus (MTG) and STG with significantly more power in auditory trials compared to audiovisual trials. This pattern emerged as early as -300 to -200 ms (peak coord:  $x = -47.2$ ,  $y = -33$ ,  $z = -4.3$ ,  $p = 0.0003$ ) and peaked during the time-range 100 to 200 ms following sound onset (peak coord:  $x = -60.8$ ,  $y = -20.5$ ,  $z = 11.4$ ,  $p = 9.58e-12$ ). The greatest proportion of significant vertices were observed from 200 to 300 ms (STG = 27.5%, MTG = 12.4%, SMG = 5.4%), strongly weighted towards the middle to posterior STG. These data suggest that the majority of theta-related activity

during audiovisual speech processing occurs following sound onset instead of in preparation for processing the auditory stimulus.

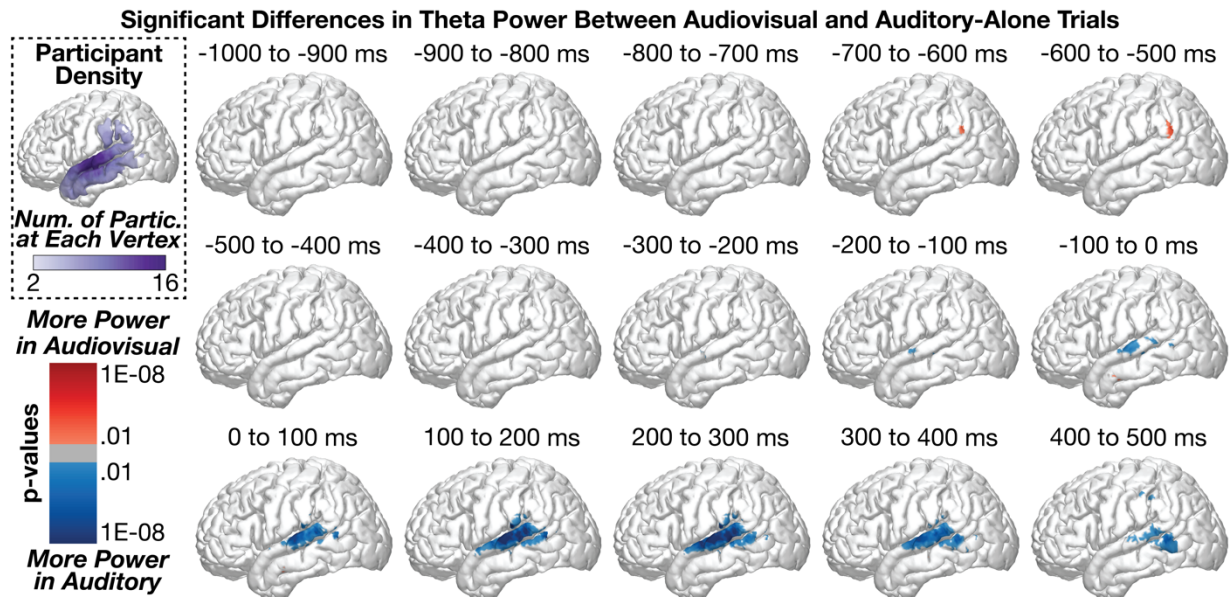


**Figure 2:** Group-level analyses comparing theta power between audiovisual and auditory-alone conditions at 100 ms time-windows (sound onset at 0 ms). Statistics conducted vertex-wise at the individual participant level and aggregated across participants using Stouffer's Z-Score method. Multiple comparisons applied across time and space using FDR. Top-left plot shows the number of participants who were included at each vertex. Congruent audiovisual stimuli elicited reduced theta power at the middle to posterior STG, peaking after the onset of the speech sound.

### 3.2 Group-Level Spatial Analyses: Beta Power

Figure 3 shows group-level differences in beta power (13 - 30 Hz) between audiovisual and auditory-alone trials. As was observed in the theta band, a small but significant difference (audiovisual > auditory) emerged from -700 to -600 ms before sound onset in the supramarginal gyrus (peak coordinates:  $x = -60.1$ ,  $y = -24.6$ ,  $z = 15$ ,  $p = 0.0054373$ ; .2% of SMG vertices were significant); no other significant audiovisual > auditory differences were observed throughout the time-series. In contrast to this initial pattern, the majority of condition differences were observed in the STG with significantly more power in auditory trials compared to audiovisual trials; this observation of reduced beta power is most consistent with *increased* beta suppression (see Section 3.5 for additional evidence). This pattern emerged as early as -400 to -300 ms (peak coord:  $x = -61.8$ ,  $y = -1$ ,  $z = -11.8$ ,  $p = 0.00013968$ ) along the anterior to middle STG/MTG and

peaked -200 to -100 ms before sound onset ( $x = -65$ ,  $y = -10$ ,  $z = 0.9$ ,  $p = 8.8008e-08$ ); the majority of significant vertices during this time-range were in the STG: STG = 16.2%, MTG = 3.1%, SMG = 2.7%. Whereas the peak activation occurred from the -200 to -100 ms time-window, the greatest proportion of significant vertices were observed in the -100 to 0 ms time-window range: STG = 20.6%, MTG = 4.9%, SMG = 2.3%. These data suggest that the majority of beta-related activity during audiovisual speech processing occurs before sound onset in contrast to the spatial and temporal pattern of results observed for theta band activity. See Section 3.7 for a direct comparison of the spatiotemporal effects between theta and beta band activity. As the differences did not emerge until after face-onset but immediately prior to sound onset (i.e., during which time preparatory visual movements were observed), we interpret these results to reflect predictive coding information along the STG (e.g., Bastos et al., 2012; Peelle and Sommers, 2015).

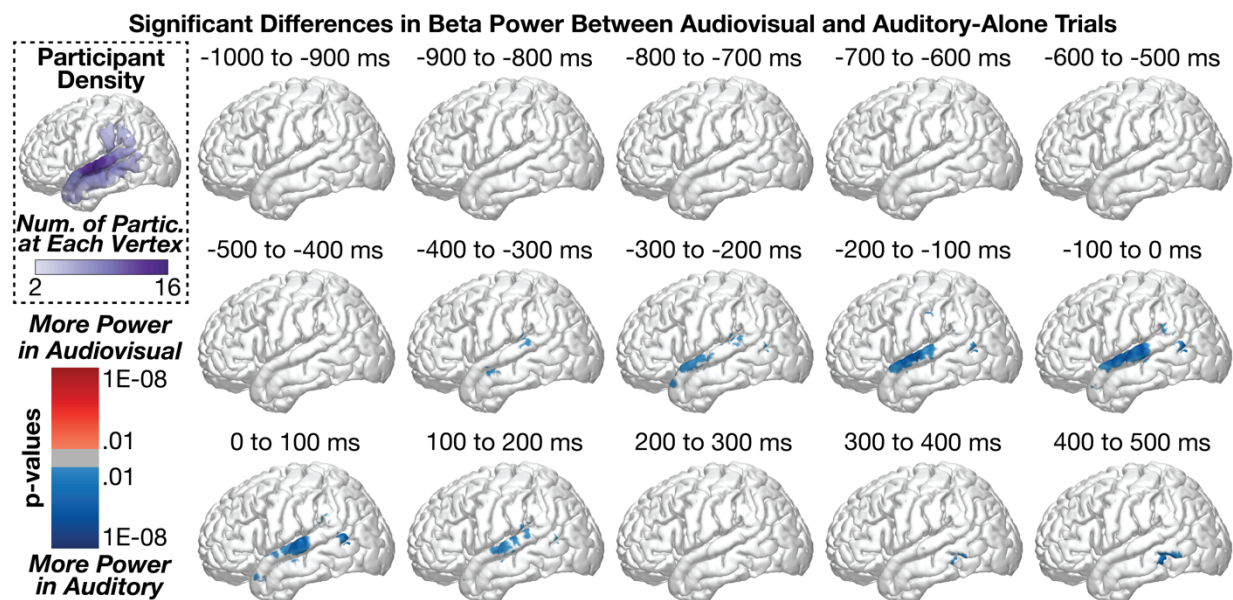


**Figure 3:** Group-level analyses comparing beta power between audiovisual and auditory-alone conditions at 100 ms time-windows (sound onset a 0 ms). Top-left plot shows the number of participants who contributed data to each vertex. audiovisual stimuli elicited greater beta suppression at the posterior STG, peaking before sound onset.

### 3.3 Group-Level Spatial Analyses: High-Gamma Power

Figure 4 shows group-level differences in high-gamma power (HGp; 70 - 150 Hz) between audiovisual and auditory-alone trials. The first significant time-points in the series were observed

in the MTG (audiovisual > auditory) beginning from -700 to -600 ms (peak coord:  $x = -55.8$ ,  $y = -63.2$ ,  $z = 8.4$ ,  $p = 1.5104e-07$ ). Small clusters of effects were observed between -600 to -100 ms (all effects reflected less than 5% of the number of vertices in each region). Beginning from -100 to 0 ms, however, we observed a strong cluster of significant differences (audiovisual > auditory) in the MTG and STG (peak coord:  $x = -57.4$ ,  $y = -66.6$ ,  $z = 9.4$ ,  $p = 8.1439e-12$ , Region = MTG, percent significant vertices in each region: STG = 8.2%, MTG = 10.1%, SMG = 1.7%). This effect persisted throughout the time-series but shifted more inferior to the MTG by 400 to 500 ms (proportion significant vertices in each region: STG = 1.4%, MTG = 12.2%, SMG = 0%). In contrast to results in the theta and beta frequency bands, HGp effects were largely restricted to the posterior STG/MTG.

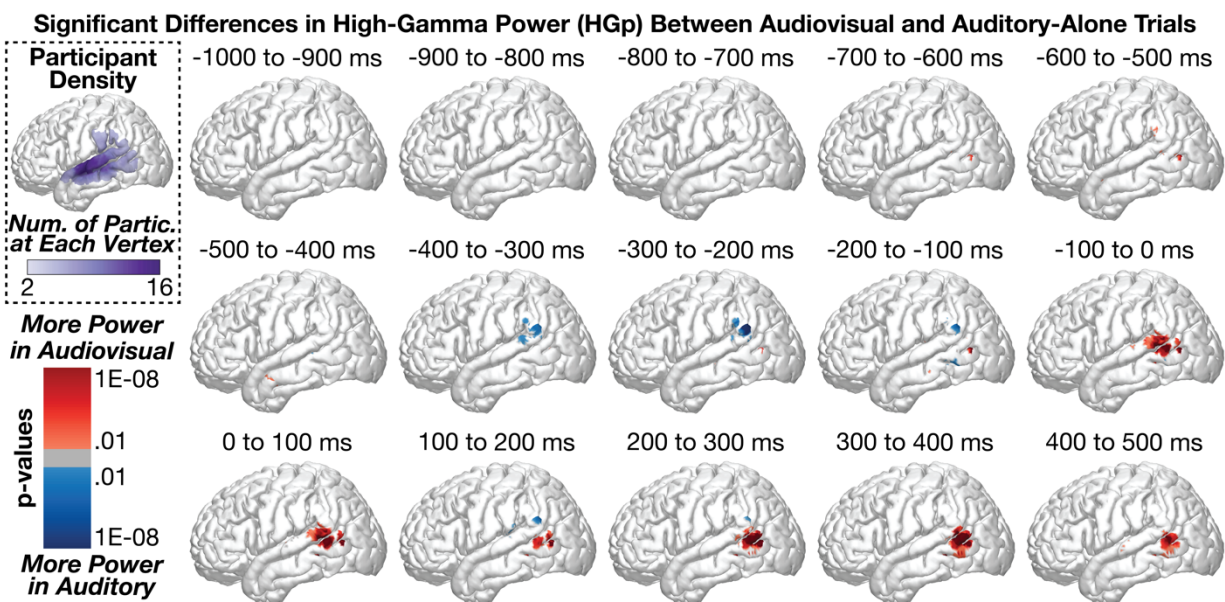


**Figure 4:** Group-level analyses comparing high gamma power (HGp) between audiovisual and auditory-alone conditions at 100 ms time-windows (sound onset a 0 ms). Top-left plot shows the number of participants who contributed data to each vertex. audiovisual stimuli elicited greater power at the posterior STG, peaking beginning before sound onset.

### 3.4 Group-Level Regional Time-Series Analyses: Theta Power

While the spatial analyses demonstrated significant patterns of activity along the STG, MTG, and SMG, this approach does not effectively allow comparisons across regions or allow the examination of interactions with time and across frequency. To model the influence of visual

speech information on auditory theta band power at the group level, we used linear mixed effects models for data aggregated into three regions of the STG (anterior, middle, and posterior regions), consistent with prior studies (Smith et al., 2013). Separate models were constructed at each time point and ROI, and multiple comparison corrections were applied. Importantly, in our estimation of condition effect (auditory-alone versus audiovisual), we modelled both random intercepts and slopes (Barr et al., 2013).

Regardless of condition, theta power within the STG increased steadily beginning before sound onset and peaked immediately after sound onset, with the strongest activity observed at the posterior STG. Consistent with the spatial analyses, we observed significant differences between audiovisual and auditory-alone conditions, with audiovisual trials leading to reduced auditory-related theta power (Figure 5). This condition difference was clearest at the posterior STG, which was significant from -93 to 500 ms (min  $p = 2.19\text{e-}06$ , peak time = 47 ms), yet also present at the middle STG, which was significant from 108 to 274 ms (min  $p = 0.030$ , peak time = 193 ms). No significant differences were observed at the anterior STG after correcting for multiple comparisons. To examine whether visual speech information differentially affected the three STG regions, we conducted group-level linear mixed-effects models with additional factors of Time and ROI (see Methods for additional information). As expected, the effect of visual

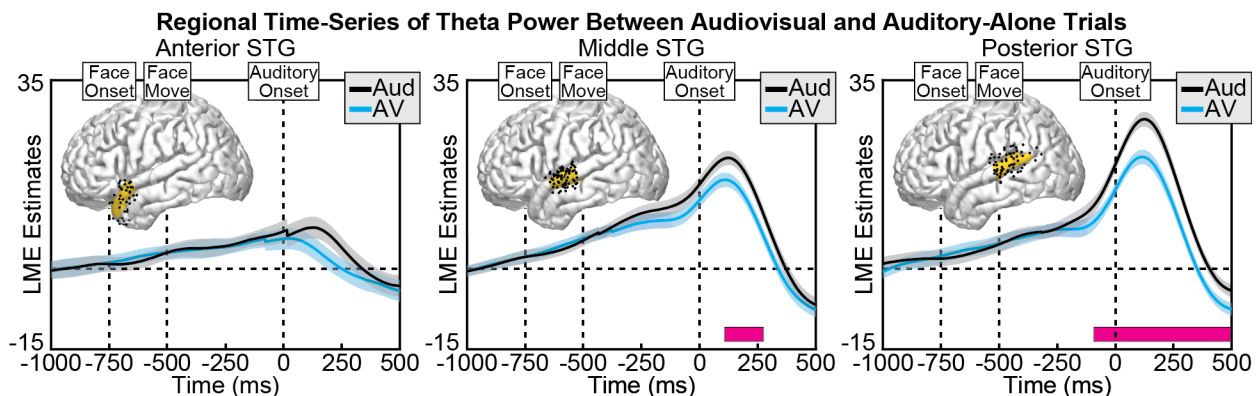


**Figure 5.** Group linear mixed-effect model (LME) estimates for each time-point of theta power in auditory-alone (black) and audiovisual (blue) trials, calculated separately at anterior (left), middle (middle), and posterior (right) regions of the STG. Shaded areas reflect 95% confidence intervals. Pink boxes reflect significant differences after correcting for multiple comparisons. Corresponding regions are highlighted on the cortical surfaces in yellow with the electrodes that contributed to the analysis shown as black dots (some depth electrodes are located beneath the surface and are not visible). Significant differences in theta power emerged largely after auditory, concentrated along the posterior STG.



information varied as a function of time (Condition x Time interaction: [ $F(1, 2.0547e+06) = 851.6, p = 3.6e-187$ ]), STG region (Condition x ROI interaction: [ $F(2, 2.0547e+06) = 28.7, p = 3.5e-13$ ]) as well as the combination of the two (Condition x Time x ROI interaction: [ $F(2, 2.0547e+06) = 147.5, p = 8.83e-65$ ]). The model with interaction terms additionally demonstrated better fit (AIC =  $7.2815e+05$ ) compared to the same model without interaction terms (AIC =  $7.4294e+05$ ). Taken together, these results indicate that visual speech information modulates auditory theta activity predominantly along the posterior STG, following sound onset.

### 3.5 Group-Level Regional Time-Series Analyses: Beta Power

Beta power in the STG showed a combination of power increases and power decreases (beta suppression), with the majority of activity focused on the mid- to posterior-STG. Across conditions, we observed significantly greater beta suppression during the audiovisual condition compared to the auditory-alone condition, peaking before sound onset at mid- to anterior STG regions (Figure 6). This condition difference was significant at both the anterior STG, significant from -311 to -195 ms (min  $p = 0.0017$ , peak time = -247 ms), and the middle STG, significant from -195 to 235 ms (min  $p = 0.0032$ , peak time = -116 ms), with no significant differences observed at the posterior STG after correcting for multiple comparisons. To examine whether the visual speech information differentially affected the three STG regions, we conducted group-level linear

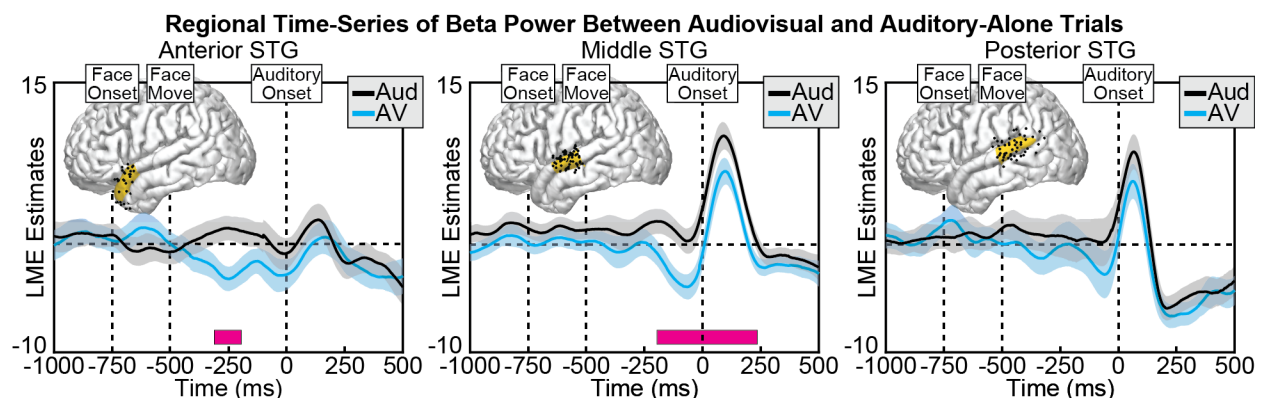


**Figure 6.** Group LME model estimates for each time-point of beta power in auditory-alone (black) and audiovisual (blue) trials, calculated separately at anterior (left), middle (middle), and posterior (right) regions of the STG. Pink boxes reflect significant differences after correcting for multiple comparisons. Corresponding regions are highlighted on the cortical surfaces in yellow with the electrodes that contributed to the analysis shown as black dots. Significant differences in beta power peaked before sound onset, concentrated in the middle to posterior STG.

mixed-effects models with additional factors of Time and ROI. As expected, the effect of visual information varied as a function of time (Condition x Time interaction: [ $F(1, 1.9693e+06) = 48.5, p = 3.25e-12$ ]), STG region (Condition x ROI interaction: [ $F(2, 1.9693e+06) = 44.2, p = 6.26e-20$ ]) but a non-significant combination of the two (Condition x Time x ROI interaction: [ $F(2, 1.9693e+06) = 2.01, p = 0.134$ ]). The model with interaction terms nevertheless demonstrated better fit (AIC =  $-1.3239e+05$ ) compared to the same model without interaction terms (AIC =  $-1.2912e+05$ ).

### 3.6 Group-Level Regional Time-Series Analyses: High-Gamma Power

In general, HGp in the STG showed auditory-related power increases that were biased towards the posterior STG. Across conditions, we observed significantly greater HGp in the audiovisual condition compared to the auditory-alone condition, occurring before sound onset and localized to the posterior STG (Figure 7). This condition difference was significant only at the posterior STG, from -45 to 24 ms (min  $p = 0.028448$ , peak time = -9 ms). No other significant differences were observed. To examine whether visual speech information differentially affected the three STG regions we conducted group-level linear mixed-effects models with additional factors of Time and ROI. As expected, the effect of visual information varied as a function of time (Condition x Time interaction: [ $F(1, 1.7919e+06) = 86.7, p = 1.266e-20$ ]), STG region (Condition

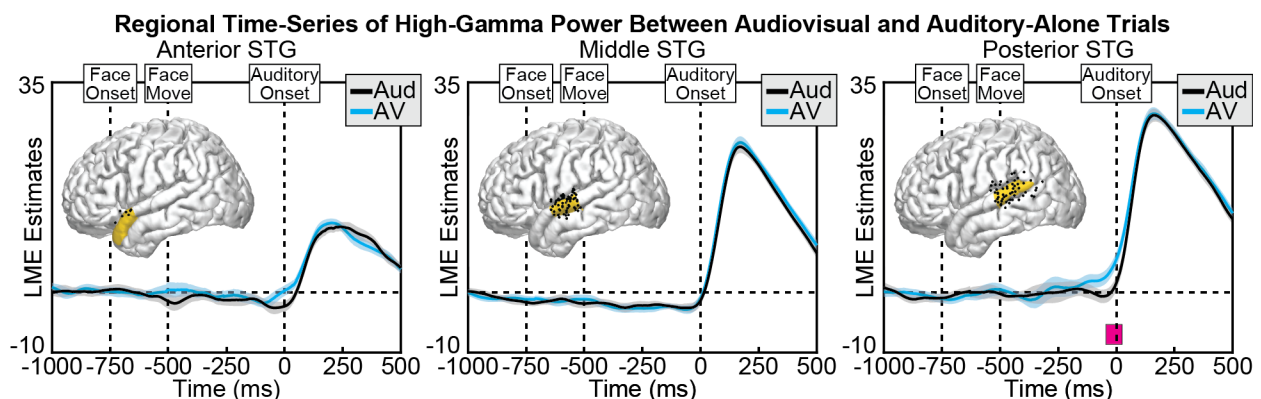


**Figure 7.** Group LME model estimates for each time-point of HGp in auditory-alone (black) and audiovisual (blue) trials, calculated separately at anterior (left), middle (middle), and posterior (right) regions of the STG. Pink boxes reflect significant differences after correcting for multiple comparisons. Corresponding regions are highlighted on the cortical surfaces in yellow with the electrodes that contributed to the analysis shown as black dots. Significant differences in HGp peaked before sound onset in the posterior STG.

x ROI interaction: [ $F(2, 1.7919e+06) = 29.6, p = 1.3e-13$ ]) as well as the combination of the two (Condition x Time x ROI interaction: [ $F(2, 1.7919e+06) = 20.0, p = 2.1e-09$ ]). The model with interaction terms additionally demonstrated better fit (AIC =  $-1.4021e+06$ ) compared to the same model without interaction terms (AIC =  $-1.1389e+06$ ).

### 3.7 Group-Level Regional Time-Series Analyses: Interactions Across Frequencies

Analyses conducted separately at each of the frequency bands demonstrated that audiovisual stimuli (compared to auditory-alone stimuli) elicited patterns of activity that occurred in putatively distinct time ranges and spatial distributions. However, to test the claim that the spatial and temporal patterns observed across the frequency bands are indeed distinct, it is necessary to model frequency band and time-points in relation to task conditions. To this end, we used group-level linear mixed-effect models that included fixed effects of task condition, frequency band, region of interest along the STG, and time, modeling both random intercepts and random slopes for trial condition. Including all frequency bands in the model yielded significant interactions of Condition x Frequency Band [ $F(2, 2.9023e+07) = 277.4, p = 2.32e-64$ ], Condition x Frequency Band x ROI [ $F(4, 2.9023e+07) = 72.7, p = 4.81e-43$ ], Condition x Frequency Band x Time [ $F(2, 2.9023e+07) = 2254.0, p = 1.21e-294$ ], and Condition x Frequency Band x ROI x Time [ $F(4, 2.9023e+07) = 397.8, p = 3.73e-163$ ]. Consistent with these significant interactions, the addition of each parameter improved model fit based on AIC. Repeating this analysis with only low-frequency signals associated with neural oscillations (theta and beta) yielded the same pattern, with significant interactions of Condition x Frequency Band [ $F(2, 2.0081e+07) = 346.7, p = 2.20e-40$ ], Condition x Frequency Band x ROI [ $F(2, 2.0081e+07) = 43.2, p = 1.90e-15$ ], Condition x Frequency Band x Time [ $F(1, 2.0081e+07) = 1645.2, p = 2.53e-121$ ], and Condition x Frequency Band x ROI x Time [ $F(2, 2.0081e+07) = 357.6, p = 9.62e-78$ ]. Again, the addition of each parameter improved model fit based on AIC. Taken together, these data demonstrate that visual speech information evokes distinct temporal and spatial patterns through theta, beta, and HGp.

### 3.8 Individual Differences in Neural Activity

While the linear mixed-effect models demonstrate effects that are present at the group level, it is important to note that highly significant condition differences were observed at individual electrodes in individual participants that deviated from these group patterns. In particular, HGp results showed greater variability across electrodes and participants than did theta and beta bands. While the most consistently observed response was increased activity before sound onset in posterior regions of the STG, this was not present in all participants or all electrodes. Figure 8 shows pairs of individual electrode responses from 5 participants, with the top row highlighting one STG electrode from that participant that demonstrated the pattern observed at the group level, and the bottom row highlighting a second STG electrode that demonstrated a different (sometimes opposite) pattern. Of note, many of the electrodes showed significantly reduced HGp to audiovisual versus auditory-alone stimuli during sound processing (100 - 200 ms); while this pattern was demonstrated in many electrodes and participants, the anatomical region varied throughout the STG and the overall pattern did not reach significance at the group level. Indeed, Participant 9 (first column) showed the opposite pattern across two electrodes, with the lower row demonstrating more HGp for *auditory* trials before sound onset.

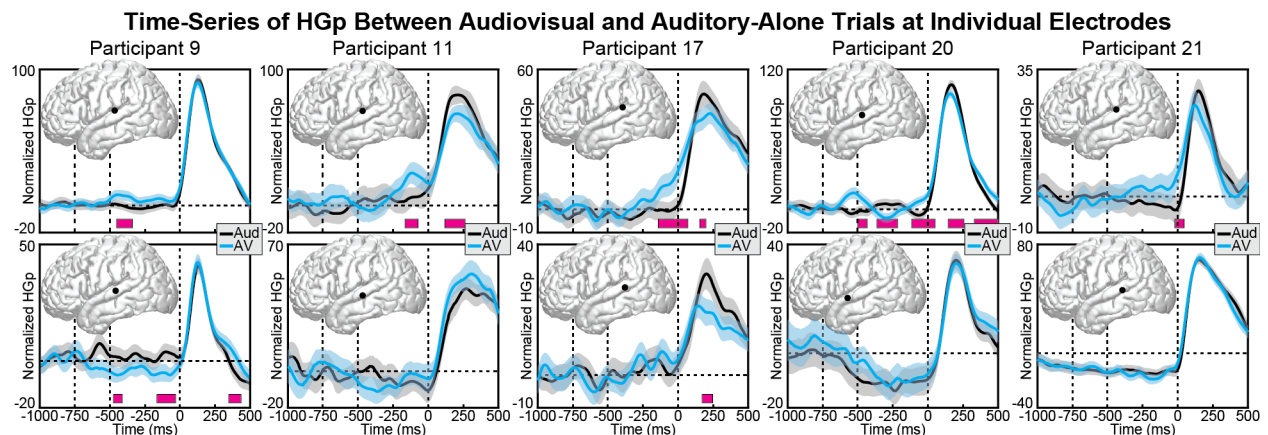


**Figure 8.** Individual participant HGp activity at audiovisual (blue) and auditory-alone (black) conditions. Each column displays data from a different participant (two electrodes per participant). Top row displays data from electrodes that showed the same pattern of HGp results observed at the group-level, with increased activity in the audiovisual condition starting before sound onset. Bottom row shows a proximal electrode that demonstrated a different (sometimes conflicting) pattern. Shaded areas reflect 95% confidence intervals. Pink boxes reflect significant differences after correcting for multiple comparisons.

## 4 Discussion

Visual signals are known to affect auditory speech processes in multiple ways. For example, lipreading signals provide high-level phonemic representations (Bourguignon et al., 2020), visual motion information can relay timing information (McGrath et al., 1985), lip closure facilitates the parsing of word-boundaries and speech rate (Chandrasekaran et al., 2009), lip-shape provides spectral information (Plass et al., 2020), and speaker identity can further enhance spatial localization and multisensory binding (Vatakis and Spence, 2007; Brang 2019). However, little research has examined the different ways in which the auditory system responds to and encodes information from these various forms of visual benefit. Indeed, a persistent challenge in identifying the various effects of audiovisual speech information has been largely methodological in nature. fMRI studies lack the temporal resolution to identify whether visual speech modulates auditory regions before, simultaneously with, or after the onset of auditory speech. On the other hand, iEEG studies face two critical shortcomings: 1. Past studies investigating audiovisual speech integration have analyzed data using single-subject designs or traditional parametric statistics making it hard to generalize the findings to the group-level and thus to the general population (Micheli et al., 2020; Besle et al., 2008; Plass et al., 2019). 2. Even while using variants of group-level analysis such as linear mixed-effects modelling, previous studies (Ozker et al., 2017; Ozker et al., 2018) have focused on HGp, which indexes local population firing rates, ignoring low-frequency oscillations which likely reflect distinct audiovisual information.

To test for the presence of separate but concurrent visual processes in auditory areas, we measured neural activity using intracranially implanted electrodes in a large number of human participants ( $n = 21$ ) during an audiovisual speech perception paradigm. These data demonstrated that at least three distinct patterns of activity occur in the STG during audiovisual speech perception relative to speech perception that occurs without corresponding visual signals. We observed (1) reduced beta power (higher beta suppression) in mid- to anterior-STG sites that peaked before sound onset, (2) increased high-gamma power localized to the posterior STG that

also peaked before sound onset, and (3) reduced theta power in mid- to posterior-STG sites that peaked after sound onset. We interpret these distinct patterns to reflect distinct neural processing in auditory regions, potentially responsible for encoding different types of visual signals that aid in auditory speech perception.

Converging behavioral and neurophysiological evidence suggests that audiovisual enhancements from audiovisual speech (e.g., better detection and faster reaction times) and visual recovery of phoneme information are subserved by two distinct mechanisms (Eskelund et al., 2011; Plass et al., 2014). This distinction may reflect a neural dissociation between predictive multisensory interactions that optimize feedforward encoding of auditory information and later feedback processes that alter auditory representations generated in the pSTS (Arnal et al., 2009; Arnal et al., 2011) and the posterior STG (Reale et al., 2007). In support of this view, both visual speech (Besle et al., 2004; Arnal et al., 2009; Van Wassenhove et al., 2005) and other anticipatory visual cues (Vroomen and Stekelenburg, 2010) can speed-up and reduce the magnitude of early physiological responses associated with auditory feedforward processing, potentially reflecting optimization of auditory encoding in accordance with temporal or acoustic constraints imposed by visual information. These early feedforward effects, which are insensitive to audiovisual congruity in speech, are temporally, spatially, and spectrally distinct from later (>300 ms) responses that are specific to crossmodally incongruent speech (Arnal et al., 2011; Van Wassenhove et al., 2005). These later incongruity-specific interactions point to a hierarchical feedback regime in which unisensory speech processing is altered in accordance with integrated audiovisual information from the pSTS (Olasagasti et al., 2015; Kayser and Logothetis, 2009) and the general speech perception areas in the STG (Mesgarani et al., 2014). These data are consistent with this dissociation, with several temporally and spatially discrete neural responses in the STG. It should also be noted that some of these patterns of activities might likely be due to attentional or non-specific effects.

Our observation of a dissociation of effects among theta and beta frequency ranges is consistent with prior EEG and physiology research suggesting these mechanisms encode different information about a visual signal (e.g., Kumar et al., 2016; Wang et al., 2017). Theta activity effectively captures ongoing auditory timing information, including rhythmic events (e.g., Schroeder et al., 2009). Conversely, beta band activity has been more strongly associated with feedback signals that may predictively encode visual information in the auditory system prior to sound onset (e.g., Engel et al., 2010). The dissociation between theta and HGp observed is particularly interesting as HGp signals have also been implicated in a predictive coding framework, such that ensembles of neurons in the posterior STG initially activate neuronal ensembles before sound onset, leading to refined population tuning and thus less HGp following sound onset (Karas et al., 2019). While this reduction in HGp during audiovisual trials was prevalent throughout many participants (see Figure 8), it was not observed at the group level, potentially due to anatomical variability in the location of the response or due to heterogeneity across participants.

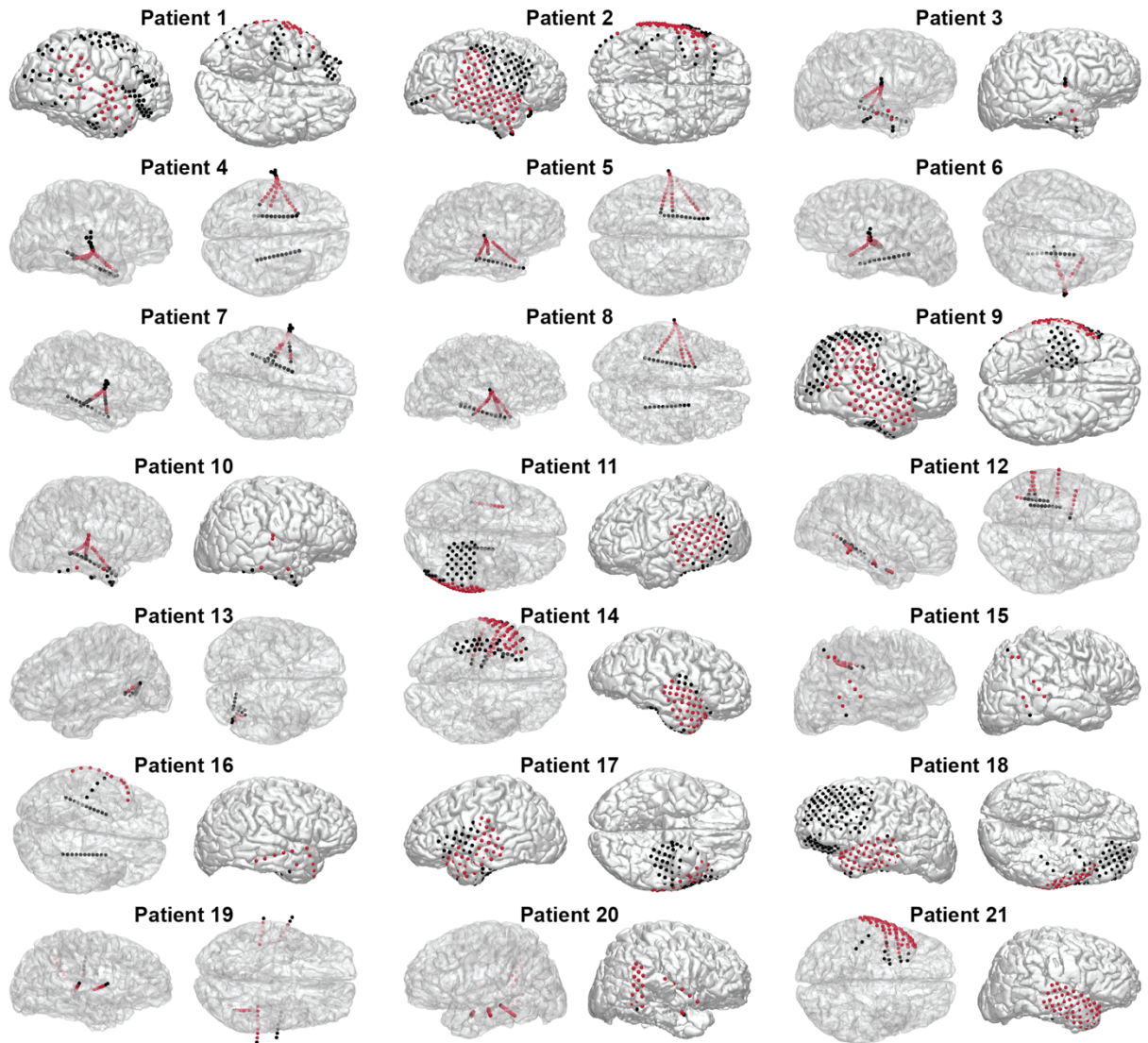
Research on the neural source of visual signals relayed to the auditory system have largely focused on the left posterior temporal sulcus (pSTS). This region demonstrates strong differences between auditory-alone and audiovisual stimuli in both fMRI and iEEG research (Beauchamp et al., 2004b; Ozer et al., 2017; Ozker et al., 2018; Okada et al., 2013), and has potential causal roles in audiovisual speech integration as revealed by lesion mapping (Hickok et al., 2018) and inhibitory transcranial magnetic stimulation (Beauchamp et al., 2010). While these data indicate that some of the information observed in the present study was likely projected through feedback pathways originating in the pSTS, particularly given its role as a center for bottom-up prediction errors in language comprehension (Lewis and Bastiaansen, 2015), it is possible that each distinct temporal/spatial pattern has a unique corresponding source. While the present study does not provide evidence as to what information is encoded within each

spatial/temporal pattern, it suggests that future research using causal measures or neural decoding could help identify the specific visual dimensions represented.

In summary, this study demonstrates that audiovisual speech integration elicits multiple distinct patterns of neural activity within the STG and adjacent cortex, occurring across separate frequencies and temporal/spatial distributions. These data suggest that visual modulation of auditory speech perception utilizes multiple mechanisms, potentially reflecting independent sources of information. Our results also indicate strong support for a hybrid family of integration models as proposed by Peele and Sommers (2015). In this account, elements from both early and late integration models are incorporated. Here, we provide support for 1) an early integration model where visual cues modulate auditory perception and 2) for a late integration model where excitatory activity in multisensory regions such as the posterior STG shape the final perception. Finally, this study additionally shows an advantage of group-level analyses of iEEG data using linear mixed-effect models, which can improve statistical validity and power, and importantly, improve generalization of results across patients and to the population at large.



## Extended Data 1-1



**Extended Data 1-1.** Individual electrode maps for each patient. Red spheres reflect auditory electrodes that met anatomical criteria and that were not rejected during pre-processing for having excessive noise.

## References:

Aarts, E., Verhage, M., Veenvliet, J. V., Dolan, C. V., and Van Der Sluis, S. (2014). A solution to dependency: using multilevel analysis to accommodate nested data. *Nature neuroscience*, 17(4), 491-496.

Arnal, L. H., Morillon, B., Kell, C. A., and Giraud, A. L. (2009). Dual neural routing of visual facilitation in speech processing. *Journal of Neuroscience*, 29(43), 13445-13453.

Arnal, L. H., Wyart, V., and Giraud, A. L. (2011). Transitions in neural oscillations reflect prediction errors generated in audiovisual speech. *Nature neuroscience*, 14(6), 797.

Bastos, A. M., Usrey, W. M., Adams, R. A., Mangun, G. R., Fries, P., and Friston, K. J. (2012). Canonical microcircuits for predictive coding. *Neuron*, 76(4), 695-711.

Beauchamp, M. S., Lee, K. E., Argall, B. D., and Martin, A. (2004a). Integration of auditory and visual information about objects in superior temporal sulcus. *Neuron*, 41(5), 809-823.

Beauchamp, M. S., Argall, B. D., Bodurka, J., Duyn, J. H., and Martin, A. (2004b). Unraveling multisensory integration: patchy organization within human STS multisensory cortex. *Nature neuroscience*, 7(11), 1190.

Beauchamp, M. S., Nath, A. R., and Pasalar, S. (2010). fMRI-Guided transcranial magnetic stimulation reveals that the superior temporal sulcus is a cortical locus of the McGurk effect. *Journal of Neuroscience*, 30(7), 2414-2417.

Bernstein, L. E., and Liebenthal, E. (2014). Neural pathways for visual speech perception. *Frontiers in Neuroscience*, 8(DEC), 386. <https://doi.org/10.3389/fnins.2014.00386>

Besle, J., Fort, A., Delpuech, C., and Giard, M. H. (2004). Bimodal speech: early suppressive visual effects in human auditory cortex. *European journal of Neuroscience*, 20(8), 2225-2234.

Besle, et al., (2008). Visual activation and audiovisual interactions in the auditory cortex during speech perception: intracranial recordings in humans. *Journal of Neuroscience*, 28(52), 14301-14310.

Bourguignon, M., Baart, M., Kapnola, E. C., and Molinaro, N. (2020). Lip-reading enables the brain to synthesize auditory features of unknown silent speech. *Journal of Neuroscience*, 40(5), 1053-1065.

Brang, D., Dai, Z., Zheng, W., and Towle, V. L. (2016). Registering imaged ECoG electrodes to human cortex: A geometry-based technique. *Journal of neuroscience methods*, 273, 64-73.

Brang, D. (2019). The Stolen Voice Illusion. *Perception*, 48(8), 649-667.

Chandrasekaran, C., Trubanova, A., Stillitano, S., Caplier, A., and Ghazanfar, A. A. (2009). The natural statistics of audiovisual speech. *PLoS computational biology*, 5(7), e1000436.

Chang, E. F., Rieger, J. W., Johnson, K., Berger, M. S., Barbaro, N. M., and Knight, R. T. (2010). Categorical speech representation in human superior temporal gyrus. *Nature neuroscience*, 13(11), 1428.

Chen, T., and Rao, R. R. (1998). Audio-visual integration in multimodal communication. *Proceedings of the IEEE*, 86(5), 837-852.

Dale, A. M., Fischl, B., and Sereno, M. I. (1999). Cortical surface-based analysis: I. Segmentation and surface reconstruction. *Neuroimage*, 9(2), 179-194.

Elliott, T. M., and Theunissen, F. E. (2009). The modulation transfer function for speech intelligibility. *PLoS comput biol*, 5(3), e1000302.

Erber, N. P. (1975). Auditory-visual perception of speech. *Journal of speech and hearing disorders*, 40(4), 481-492.

Fischl, B., Sereno, M. I., and Dale, A. M. (1999). Cortical surface-based analysis: II: inflation, flattening, and a surface-based coordinate system. *Neuroimage*, 9(2), 195-207.

Hickok, G., Rogalsky, C., Matchin, W., Basilakos, A., Cai, J., Pillay, S., and Binder, J. (2018). Neural networks supporting audiovisual integration for speech: A large-scale lesion study. *Cortex*, 103, 360-371.

Engel, A. K., and Fries, P. (2010). Beta-band oscillations—signalling the status quo?. *Current opinion in neurobiology*, 20(2), 156-165.

Eskelund, K., Tuomainen, J., and Andersen, T. S. (2011). Multistage audiovisual integration of speech: Dissociating identification and detection. *Experimental Brain Research*, 208(3), 447-457.

Groppe, D. M., Urbach, T. P., and Kutas, M. (2011). Mass univariate analysis of event-related brain potentials/fields II: Simulation studies. *Psychophysiology*, 48(12), 1726-1737.

Hullett, P. W., Hamilton, L. S., Mesgarani, N., Schreiner, C. E., and Chang, E. F. (2016). Human superior temporal gyrus organization of spectrotemporal modulation tuning derived from speech stimuli. *Journal of Neuroscience*, 36(6), 2014-2026.

Kadipasaoglu, C. M., Baboyan, V. G., Conner, C. R., Chen, G., Saad, Z. S., and Tandon, N. (2014). Surface-based mixed effects multilevel analysis of grouped human electrocorticography. *Neuroimage*, 101, 215-224.

Kadipasaoglu, C. M., Forseth, K., Whaley, M., Conner, C. R., Rollo, M. J., Baboyan, V. G., and Tandon, N. (2015). Development of grouped icEEG for the study of cognitive processing. *Frontiers in psychology*, 6, 1008.

Karas, P. J., Magnotti, J. F., Metzger, B. A., Zhu, L. L., Smith, K. B., Yoshor, D., and Beauchamp, M. S. (2019). The visual speech head start improves perception and reduces superior temporal cortex responses to auditory speech. *Elife*, 8, e48116.

Kayser, C., and Logothetis, N. K. (2009). Directed interactions between auditory and superior temporal cortices and their role in sensory integration. *Frontiers in integrative neuroscience*, 3, 7.

Kleiner M, Brainard D, Pelli D, 2007, "What's new in Psychtoolbox-3?" *Perception* 36 ECVF Abstract Supplement

Kumar, G. V., Halder, T., Jaiswal, A. K., Mukherjee, A., Roy, D., and Banerjee, A. (2016). Large scale functional brain networks underlying temporal integration of audio-visual speech perception: An EEG study. *Frontiers in psychology*, 7, 1558.

Lazic, S. E. (2010). The problem of pseudoreplication in neuroscientific studies: is it affecting your analysis?. *BMC neuroscience*, 11(1), 5.

Lazic, S. E., Clarke-Williams, C. J., and Munafò, M. R. (2018). What exactly is 'N' in cell culture and animal experiments?. *PLoS Biology*, 16(4), e2005282.

Lega, B., Germi, J., and Rugg, M. D. (2017). Modulation of oscillatory power and connectivity in the human posterior cingulate cortex supports the encoding and retrieval of episodic memories. *Journal of Cognitive Neuroscience*, 29(8), 1415-1432.

Lewis, A. G., and Bastiaansen, M. (2015). A predictive coding framework for rapid neural dynamics during sentence-level language comprehension. *Cortex*, 68, 155-168.

Mesgarani, N., Cheung, C., Johnson, K., and Chang, E. F. (2014). Phonetic feature encoding in human superior temporal gyrus. *Science*, 343(6174), 1006-1010.

McGrath, M., and Summerfield, Q. (1985). Intermodal timing relations and audio-visual speech recognition by normal-hearing adults. *The Journal of the Acoustical Society of America*, 77(2), 678-685.

Micheli, C., Schepers, I. M., Ozker, M., Yoshor, D., Beauchamp, M. S., and Rieger, J. W. (2020). Electro-corticography reveals continuous auditory and visual speech tracking in temporal and occipital cortex. *European Journal of Neuroscience*, 51(5), 1364-1376.

Okada, K., Venezia, J. H., Matchin, W., Saberi, K., and Hickok, G. (2013). An fMRI study of audiovisual speech perception reveals multisensory interactions in auditory cortex. *PLoS one*, 8(6), e68959.

Ozker, M., Schepers, I. M., Magnotti, J. F., Yoshor, D., and Beauchamp, M. S. (2017). A double dissociation between anterior and posterior superior temporal gyrus for processing audiovisual speech demonstrated by electrocorticography. *Journal of cognitive neuroscience*, 29(6), 1044-1060.

Ozker, M., Yoshor, D., and Beauchamp, M. S. (2018). Converging evidence from electrocorticography and BOLD fMRI for a sharp functional boundary in superior temporal gyrus related to multisensory speech processing. *Frontiers in human neuroscience*, 12, 141.

Olasagasti, I., Bouton, S., and Giraud, A. L. (2015). Prediction across sensory modalities: A neurocomputational model of the McGurk effect. *Cortex*, 68, 61-75.

Peelle, J. E., and Sommers, M. S. (2015). Prediction and constraint in audiovisual speech perception. *Cortex*, 68, 169-181.

Plass, J., Guzman-Martinez, E., Ortega, L., Grabowecy, M., and Suzuki, S. (2014). Lip reading without awareness. *Psychological science*, 25(9), 1835-1837.

Plass, J., Brang, D., Suzuki, S., and Grabowecky, M. (2019). Vision Perceptually Restores Auditory Spectral Dynamics in Speech.

Plass, J., Brang, D., Suzuki, S., and Grabowecky, M. (2020). Vision perceptually restores auditory spectral dynamics in speech. *Proceedings of the National Academy of Sciences*, 117(29), 16920-16927.

Reale, R. A., Calvert, G. A., Thesen, T., Jenison, R. L., Kawasaki, H., Oya, H., ... and Brugge, J. F. (2007). Auditory-visual processing represented in the human superior temporal gyrus. *Neuroscience*, 145(1), 162-184.

Schroeder, C. E., Lakatos, P., Kajikawa, Y., Partan, S., and Puce, A. (2008). Neuronal oscillations and visual amplification of speech. *Trends in cognitive sciences*, 12(3), 106-113.

Schroeder, C. E., and Lakatos, P. (2009). Low-frequency neuronal oscillations as instruments of sensory selection. *Trends in neurosciences*, 32(1), 9-18.

Smith, E., Duede, S., Hanrahan, S., Davis, T., House, P., and Greger, B. (2013). Seeing is believing: neural representations of visual stimuli in human auditory cortex correlate with illusory auditory perceptions. *PLoS One*, 8(9), e73148.

Stouffer, S. A., Suchman, E. A., DeVinney, L. C., Star, S. A., and Williams, R. M., Jr. (1949). *The American Soldier: Adjustment During Army Life* (Vol. 1). Princeton, NJ: Princeton University Press.

Van Wassenhove, V., Grant, K. W., and Poeppel, D. (2005). Visual speech speeds up the neural processing of auditory speech. *Proceedings of the National Academy of Sciences*, 102(4), 1181-1186.

Vatakis, A., and Spence, C. (2007). Crossmodal binding: Evaluating the “unity assumption” using audiovisual speech stimuli. *Perception and psychophysics*, 69(5), 744-756.

Vroomen, J., and Stekelenburg, J. J. (2010). Visual anticipatory information modulates multisensory interactions of artificial audiovisual stimuli. *Journal of Cognitive Neuroscience*, 22(7), 1583-1596.

Wang, L., Wang, W., Yan, T., Song, J., Yang, W., Wang, B., ... and Wu, J. (2017). Beta-band functional connectivity influences audiovisual integration in older age: an EEG study. *Frontiers in aging neuroscience*, 9, 239.

Wang, X. J. (2010). Neurophysiological and computational principles of cortical rhythms in cognition. *Physiological reviews*, 90(3), 1195-1268.